remote sensing

MDPI

Article

Assessing the Effects of Land-Use Types in Surface Urban Heat Islands for Developing Comfortable Living in Hanoi City

Nguyen Thanh Hoan [1,2], Yuei-An Liou [3,*], Kim-Anh Nguyen [1,3,*], Ram C. Sharma [4], Duy-Phien Tran [1], Chia-Ling Liou [5] and Dao Dinh Cham [1,2]

1 Institute of Geography, Vietnam Academy of Science and Technology, 18-Hoang Quoc Viet, Hanoi 100000, Vietnam; hoanrs@gmail.com (N.T.H.); duyphien.11092004@gmail.com (D.-P.T); chamvdl@gmail.com (D.D.C.)
2 Vietnam Academy of Science and Technology, Graduate University of Science and Technology, 18-Hoang Quoc Viet, Hanoi 100000, Vietnam
3 Center for Space and Remote Sensing Research, National Central University, No. 300, Jhongda Rd., Jhongli Dist., Taoyuan City 32001, Taiwan
4 Department of Informatics, Tokyo University of Information Sciences, 4-1 Onaridai, Wakaba-ku, Chiba 265-8501, Japan; sharma@rsch.tuis.ac.jp
5 Department of Horticulture, National Chung Hsing University, Taichung 42049, Taiwan; a0983433519@gmail.com
* Correspondence: yueian@csrsr.ncu.edu.tw (Y.-A.L.); nguyenrose@csrsr.ncu.edu.tw (K.-A.N.); Tel.: +886-3-4227151 (ext. 57631) (Y.-A.L.)

Received: 23 October 2018; Accepted: 4 December 2018; Published: 6 December 2018

Abstract: Hanoi City of Vietnam changes quickly, especially after its state implemented its Master Plan 2030 for the city's sustainable development in 2011. Then, a number of environmental issues are brought up in response to the master plan's implementation. Among the issues, the Urban Heat Island (UHI) effect that tends to cause negative impacts on people's heath becomes one major problem for exploitation to seek for mitigation solutions. In this paper, we investigate the land surface thermal signatures among different land-use types in Hanoi. The surface UHI (SUHI) that characterizes the consequences of the UHI effect is also studied and quantified. Note that our SUHI is defined as the magnitude of temperature differentials between any two land-use types (a more general way than that typically proposed in the literature), including urban and suburban. Relationships between main land-use types in terms of composition, percentage coverage, surface temperature, and SUHI in inner Hanoi in the recent two years 2016 and 2017, were proposed and examined. High correlations were found between the percentage coverage of the land-use types and the land surface temperature (LST). Then, a regression model for estimating the intensity of SUHI from the Landsat 8 imagery was derived, through analyzing the correlation between land-use composition and LST for the year 2017. The model was validated successfully for the prediction of the SUHI for another hot day in 2016. For example, the transformation of a chosen area of 161 ha (1.61 km^2) from vegetation to built-up between two years, 2016 and 2017, can result in enhanced thermal contrast by 3.3 °C. The function of the vegetation to lower the LST in a hot environment is evident. The results of this study suggest that the newly developed model provides an opportunity for urban planners and designers to develop measures for adjusting the LST, and for mitigating the consequent effects of UHIs by managing the land use composition and percentage coverage of the individual land-use type.

Keywords: land surface temperature; urban heat island; surface urban heat island; land use; land management unit

1. Introduction

In the context of climate change and global warming, it is important to monitor the signatures of urban heat islands (UHIs) and to understand their impacts on ecosystems and human health. UHI arises from the phenomenon of relatively higher temperature in the urban center over its surrounding rural environment. The phenomenon behind UHI has been studied for a long time. It was first described by Luke Howard in the 1810s [1]. From 1964 to 1968, Bornstein [2] used a helicopter to study the UHI of New York City, and determined the effect of UHI in both vertical and horizontal directions. The results display a maximum intensity of UHI near the ground surface, and a decrease to zero at a height of 300 m [2]. Ackerman [3] studied the diurnal and seasonal variations of UHI in Chicago, recording an increase—averaging 1.85 °C—in temperature inside the city most of the time. Since the 1990s, 3D models have been developed to examine the effects of UHI in Tokyo, Japan, using satellite and land survey data [4]. In Nagoya, Japan, seasonal changes pertaining to UHI were analyzed using Landsat and ASTER images taken during the day, as well as at night, which were modeled to determine whether or not the heat fluxes are natural or artificial [5]. In Washington, the surface temperature of the city center was found to be higher than the surrounding vegetative areas by up to 10 °C [6]. These studies indicated that vegetation cover plays a key role in minimizing the UHI effect. The minimization of the UHI effect tends to be beneficial to the community because it may result in the enhancement of dangerous natural phenomena, in addition to its impacts on ecosystems and human health. For example, it has been reported that the UHI effect may alter the precipitation [7], characteristics of cloud-to-ground lightning activities through increased aerosols [8,9] and their enhancement [10,11] in response to urbanization, and modify the environmental and regional climate by reshaping the boundary layer and land–sea circulation [12].

Many other studies also demonstrated correlations between UHI and land-use composition in a city. Weng et al. [13] reported a correlation between the surface temperature and vegetation in Indianapolis, USA. Chen et al. [14] examined the relationship between UHI and land-use change, in certain cities of the Guangdong Province in Southeast China, using Landsat images from 1990 to 2000. A similar study on the relationship between UHI, land-use change, and population density was also conducted in Nagpur, India [15]. Other studies relevant to UHI effects were also conducted [16–20]. These studies provide similar conclusions that urban temperatures are highly correlated with land-use composition (water, vegetation, built-up, among others) in the cities. Due to easy access and wall-to-wall continuous coverage, LST derived from thermal infrared remote sensors are one of the most commonly used indicators for surface UHI (SUHI) analysis [21–24]. In this study, the SUHI is defined as the magnitude of the temperature differentials between any two land-use types, a more general way than that which is typically adopted in the literature. From the physical point of view, LST and air temperature are different entities, while strong correlations were found between them by many researchers in the literature [21,25,26].

More recently, Deilami et al. [27] provided a systematic and overarching review of different spatiotemporal factors that affect the UHI effect. It is indicated that the UHI effect can be considered as a critical factor contributing to heat-related mortalities, and unpredictable climatic changes. Lai et al. [28] were concerned with the quality control of the satellite data for investigating the SUHI. They used eighty-six major cities across mainland China, and analyzed SUHI intensity (SUHII) derived from Moderate Resolution Imaging Spectroradiometer (MODIS) LST data. Their findings suggested the need to be extremely cautious when using LST product-based SUHIIs to interpret SUHIs. Li et al. [29] presented a new method to quantify the SUHI. They were concerned with the effective evaluation of potential heat risk. A new approach was proposed to quantify the SUHII by using the relationship between MODIS LST and impervious surface areas (ISA). The calculated SUHII shows high values in summer and during the day than in winter and at night. Despite a great effort being devoted to study the UHI and SUHI in the major cities of the world, fewer investigations have been conducted to solve the associated problems for developing countries such as Southeast Asian countries, among which Vietnam implemented a Master Plan 2030 for its capital, Hanoi, in 2011. How will the Master Plan

impact Hanoi's overall environmental conditions? Nam et al. [30] evaluated the influence of UHI under the Hanoi Master Plan 2030 on the energy consumption for space cooling in residential buildings. They found that the increments in built-up areas were larger than those in existing built-up areas, and that the cooling load in an apartment is approximately half of that in a detached house, which itself approximately half of that in a row house. It was also observed that although sensible cooling loads increased with the increase in outdoor temperature, the latent cooling loads decreased due to the decrease in absolute humidity and the increase in air temperature. Trihamdani et al. [31] assessed the UHI effects in the city under the present land use conditions, as well as those conditions proposed by the Hanoi Master Plan 2030 through numerical simulation, using Weather Research and Forecasting (WRF). They found that the peak air temperature in the built-up areas (approximately 1 °C higher at the maximum) was not significantly modified, but high temperature areas, with temperatures of 40–41 °C, would expand widely over the new built-up areas. They also stressed that the number of hotspots increased further when the strategic green spaces in the master plan were not taken into account.

Based on the literature survey, state-of-the-art of correlations between UHI or SUHI and land-use composition are being widely analyzed in the recent years. In contrast, the study of UHI or SUHI with respect to Hanoi City Master Plan 2030 is rather limited; for example, about spatial energy consumption [30], assessment of UHI effects based on WRF simulations [31]. Then, what would be the most updated status of land use change with respect to the city Master Plan? What would be the impact on the thermal signatures? What possible measures can the city take to mitigate UHI? Therefore, the objectives of this research are to (i) assess the land use changes in Hanoi, (ii) assess the quantitative relationships between the composition of the main land-use types and SUHI in Hanoi, (iii) analyze the effects of land-use composition on SUHI on an extremely hot day, (iv) derive a regression model for the prediction of SUHI, and (v) suggest the measures applicable for minimizing the SUHI impacts on human health, due to increased urban temperature.

2. Methodology

2.1. Study Area

Inner Hanoi was chosen as our study site. It is situated in the capital city of Vietnam, encompassing an area of 160 km^2 (yellow polygon in Figure 1c). The studied location mainly comprises built-up areas, vegetation covers, and water bodies. The geographical location of the study area from a global view, to the national scale, to the regional scale is illustrated in Figure 1. The figure also depicts the boundary of Hanoi City before and after 2008, a composited Landsat 8 satellite image acquired on 4 June 2017, and locations of the meteorological stations Lang (yellow) and Ha Dong (orange) were used to acquire air temperature data.

In terms of population, Hanoi is inhabited by more than 7.7 million people (whole Hanoi as shown in Figure 1b) and it has a high population density (12,340 people/km^2) in urban districts in 2015. As for climate, it is located in a tropical belt so that its summer lasts from May to August with a hot and humid atmosphere, abundant rainfall, and an average temperature of 29 °C. On average, July is the hottest month. Its annual average rainfall is 1680 mm, and the average temperature 23.6 °C.

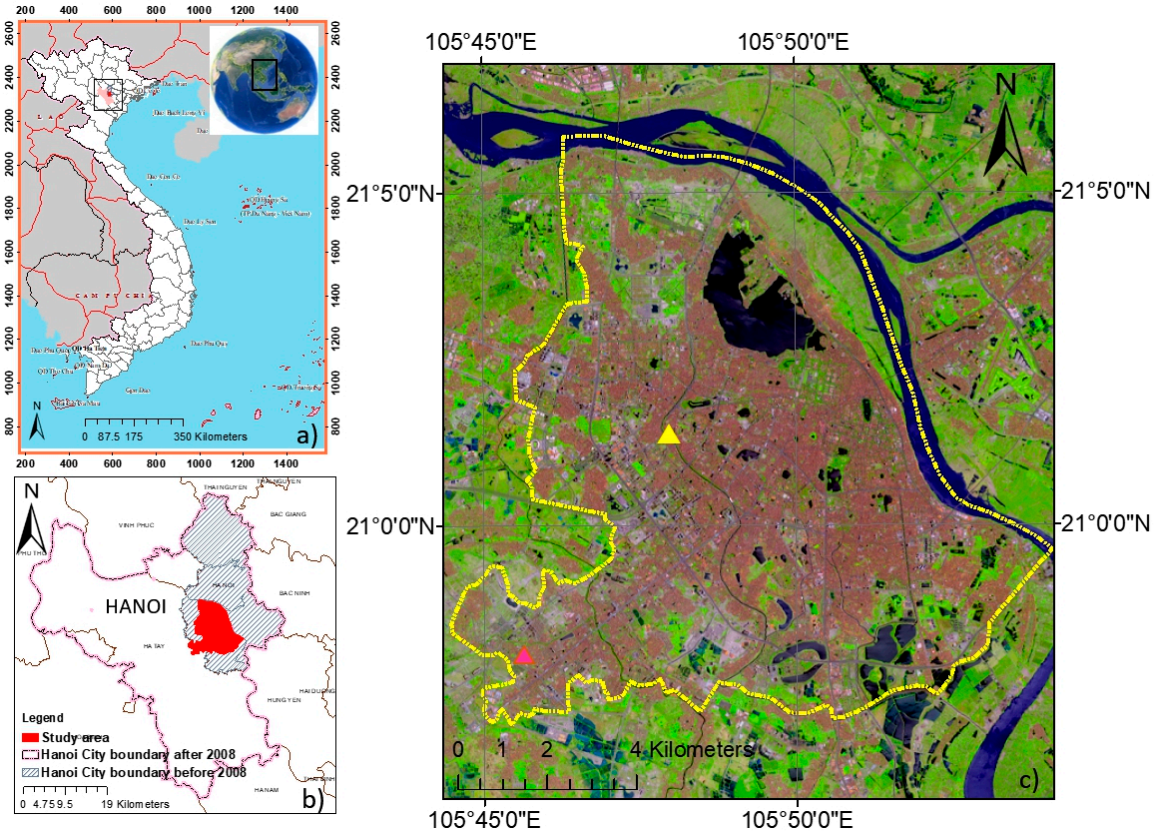

Figure 1. Location of the study area: (**a**) Location of the study area in Vietnam; (**b**) detail of the study area with the boundary of Hanoi City before and after 2008; (**c**) inner Hanoi city (yellow polygon) on the composited Landsat 8 satellite image acquired on 4 June 2017, and locations of the meteorological stations Lang (yellow) and Ha Dong (orange) used to acquire air temperature data.

2.2. Air Temperature Data

The air temperature (°C) of the monthly hottest days observed at two meteorological stations (Lang and Ha Dong as shown in Figure 1) in Hanoi in 2016 and 2017 are listed in Table 1. Therefore, the days with the hottest air temperature are selected and considered as having the most negative effects on human health that are associated with UHI effect. From Table 1, it shows that the monthly hottest days are 2 June and 4 June in 2016 and 2017, respectively.

Table 1. Maximum monthly air temperatures (°C) in Hanoi in 2016 and 2017.

Year Station	Month												Max	In Day
	1	2	3	4	5	6	7	8	9	10	11	12		
2016_Lang	29.7	33.3	26.9	34.1	36.9	**40.4**	39.2	37.5	36.3	34.3	32.2	29.5	**40.4**	**2nd**
2017_Lang	27.9	28.8	30.5	35.3	35.0	**41.8**	38.9	37.6	36.7	33.6	33.6	25.9	**41.8**	**4th**
2016_Ha Dong	30.5	33.0	26.8	32.7	36.7	**39.3**	38.5	37.4	36.1	34.0	32.0	29.5	**39.3**	**2nd**
2017_Ha Dong	27.5	29.2	29.8	35.7	35.5	**42.5**	38.2	37.0	36.0	33.3	33.0	25.8	**42.5**	**4th**

2.3. Acquisition and Pre-Processing of Satellite Data

We acquired the Landsat 8 OLI (Operational Land Imager) and TIRS (Thermal Infrared Sensor) images for the same day (4 June 2017; scene ID: LC08_L1TP_127045_20170604_20170615_01_T1), when Hanoi experienced the greatest heat wave in recent 40 years. On that day, the air temperature in Hanoi reached up to 42 °C. Since Landsat 8 images were not available for 2 June 2016, the hottest day of 2016, we acquired the Landsat 8 OLI and TIRS images for the second hottest day of 1 June 2016

(scene ID: LC08_L1TP_127045_20160601_20170324_01_T1). For simplicity, 1 June is still named as the hottest day in 2016 hereafter, in the paper. On that day, the air temperature in Hanoi reached up to 39 °C. The Landsat 8 image of 2016 are later used to validate the models that are developed from the Landsat 8 images of 2017. The OLI data were converted into Top-Of-Atmosphere (TOA) spectral reflectance, applying the rescaling coefficients that are available in the metadata file. The Landsat 8 images utilized for the study area are cloud-free.

2.4. Land-Use Mapping and Validation

We adopted the ISODATA-based (Iterative Self-Organized Data analysis) unsupervised classification approach for mapping the three major land-use types, built-up area, water body, and vegetation cover, which are prevalent in inner Hanoi City. We carried out tasseled cap transformation for the Landsat 8 OLI images, and calculated three tasseled cap indices, Greenness, Wetness, and Brightness, following the methodology and transformation coefficients (Table 2) provided by Baig et al. [32].

These three tasseled cap indices were used for ISODATA-based clustering and unsupervised mapping of the land-use types for the years 2016 and 2017. Four main land-use types, including built-up, vegetation, water, and others (others mean that the pixels (regions) are mixed with built-up, vegetation, and water) were mapped. For validation, we made a common map (changed and un-changed areas) between 1 June 2016 and 4 July 2017, including four classes: built-up, vegetation, water, and others & changes. The changed areas are not stable pixels (and also needed to be checked). We chose 100 geo-location points belonging to the un-changed area of each class (built-up, Vegetation, and water) plus the others & changes areas, to validate the classification results. A total of 300 points (for three target classes) were selected. The random points were checked through visual interpretation of Google Earth images and Google Map, acquired in June 2016 and August 2017, respectively. The distribution of the chosen points is displayed in Figure 2.

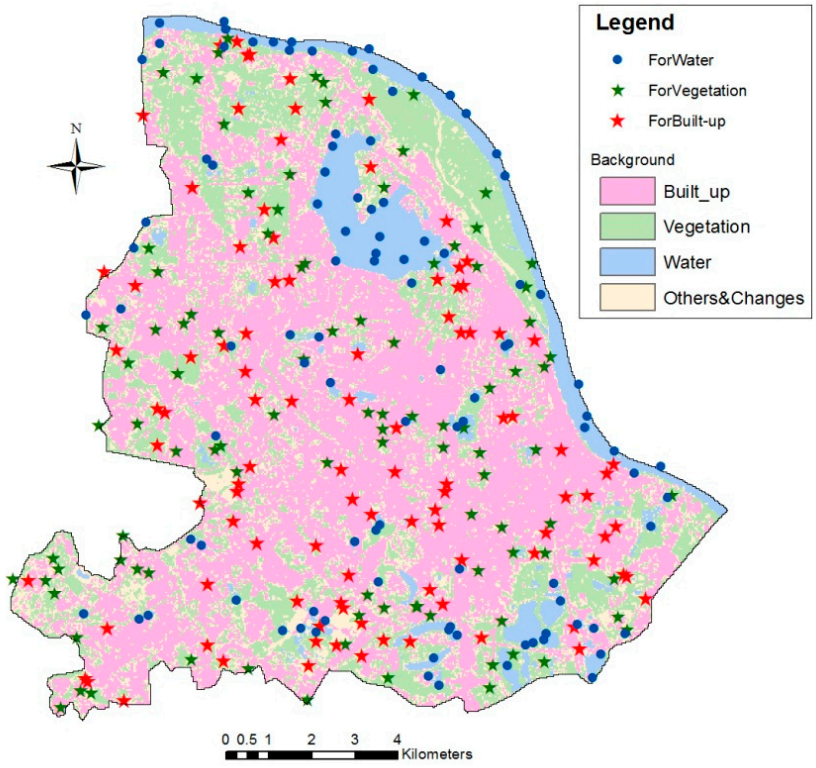

Figure 2. Distribution of the ground truth points on a common area map chosen in the research.

Table 2. Tasseled cap transformation coefficients for Landsat 8 at-satellite reflectance of six bands: Blue, Green, red, near-infrared (NIR), shortwave infrared (SWIR 1), and shortwave infrared (SWIR 2) (adopted from Baig et al. [32]).

Tasseled Cap Indexes	Landsat 8 Bands					
	Blue (Band 2)	**Green (Band 3)**	**Red (Band 4)**	**NIR (Band 5)**	**SWIR 1 (Band 6)**	**SWIR 2 (Band 7)**
Brightness	0.3029	0.2786	0.4733	0.5599	0.508	0.1872
Greenness	−0.2941	−0.243	−0.5424	0.7276	0.0713	−0.1608
Wetness	0.1511	0.1973	0.3283	0.3407	−0.7117	−0.4559

2.5. Mapping of Land Surface Temperature

According to the United States Geological Survey (USGS), Thermal infrared sensor (TIRS) bands of Landsat 8 have been affected by stray light from far out-of-field since its launch in 2013. A new stray light correction algorithm (SLCA) has been implemented into the USGS ground system since February 2017 and applied to reprocess historical Landsat 8 images. After SLCA implementation, Wang and Lentilucci [33] had a study to compare Landsat 8 TIRS Stray Light Correction with Multi-Sensor Measurements. It was concluded that the maximum difference in a temperature varies from 0.5% to 0.7% only. García-Santos et al. [34] validated the SLCA implementation using in situ LST measurements and three different LST estimation method algorithms (radiative transfer equation (RTE), single-channel algorithms (SCA), and split-window algorithms (SWA)) were applied for 21 scenes of Landsat 8 images. The in situ measured site is composed of different types of land covers, such as buildings, asphalt roads, vegetation regions, and so on. The study concluded that the SWA shows the best result for LST calculation from the Landsat 8 image with the lowest root mean square error (RMSE) (within 1.6–2 K). Therefore, the SWA was selected to calculate the LST for this study.

LST maps were generated by using the thermal infrared bands 10 and 11, which are available in the Landsat 8 TIRS images (1 June 2016 and 4 June 2017). We applied the SWA (Equation (1)) adopted from the literature [35,36] for the generation of the LST maps:

$$\mathrm{LST} = T_i + c1(T_i - T_j) + c2(T_i - T_j)^2 + c_0 + (c3 + c4w)\,(1 - \varepsilon) + (c5 + c6w)\,\Delta\varepsilon \quad (1)$$

where T_i and T_j are the at-sensor brightness temperatures at the thermal infrared bands i and j (in Kelvins), respectively, ε is the mean emissivity, $\varepsilon = 0.5(\varepsilon_i + \varepsilon_j)$; $\Delta\varepsilon$ is the emissivity difference, $\Delta\varepsilon = (\varepsilon_i - \varepsilon_j)$; w is the total atmospheric water vapor content (in g·cm^{-2}); and $c0$ to $c6$ are SW coefficients to be determined from simulated data.

T_i and T_j were calculated on the basis of the following formula (Equation (2)):

$$T = \frac{K_2}{Ln\left(\frac{K_1}{L_\lambda} + 1\right)} \quad (2)$$

where T is at-sensor brightness temperatures; L_λ is TOA spectral radiance in W/(m^2 ster μm); K_1 and K_2 are the pre-launch calibration constants (from metadata file of Landsat 8 image).

The TOA spectral radiance (L_λ) (in Equation (2)) was calculated from the radiance rescaling factors provided in the metadata file, applying the following formula (Equation (3)):

$$L_\lambda = M_L Q_{cal} + A_L \quad (3)$$

where M_L is the band-specific multiplicative rescaling factor; A_L is the band-specific additive rescaling factor; Q_{cal} are the quantized and calibrated standard product pixel digital numbers (DN).

The land surface emissivity (ε) was estimated from the Landsat 8 imagery using the Normalized Difference Vegetation Index (NDVI) threshold method [37]. The total atmospheric water vapor

content coefficient was obtained from NASA's Atmospheric Correction Parameter Calculator (http://atmcorr.gsfc.nasa.gov/) [38]. At the location of Hanoi (N21.00, E105.83), the total atmospheric water vapor was 5.17 g·cm^{-2} for 4 June 2017, and 5.31 g·cm^{-2} for 1 June 2016. The coefficients $c0$–$c6$ in Equation (1) were determined from the simulated data provided by Jimenez-Munoz et al. [36]. It was found that the mean error of the LST was less than 1.5 K. The original LST calculated from the Equation (1) is in Kelvin degrees. The LST was converted to Celsius degrees for regression calculation.

2.6. Preparation of Statistical Datasets

The 30 m resolution land-use and LST maps of the years 2016 and 2017 produced in the research were used to prepare statistical datasets for inner Hanoi City. We applied the moving window method with varying window sizes, from 120 × 120 m (4 × 4 pixels) to 570 × 570 m (19 × 19 pixels), for the preparation of the datasets. Note that the LST data have a native pixel size of 100 m (resampled by USGS at 30 m), and the window averaging worsens the LST resolution and the ability to capture details in a heterogeneous area. The aim of the moving window (5 × 5 pixels) throughout the study area is to gather a sufficient number of samples (as large as 7770) for the statistical analysis, and selection of window size for further analysis. A "window" with a size and shape of interest is moved over the data with a moving distance that is equal to the window's width. For each window, the percentage coverage of the land-use types, urban built-up (%U), vegetation cover (%V), and water body (%W), were calculated. We also calculated the mean land surface temperature (μLST) for each window. The statistical datasets of 2016 were used for the validation of the model derived with 2017 datasets.

2.7. Regression Analysis, Modeling, and Validation

The statistical datasets constituting land-use composition (%U, %V, and %W) and μLST with varying window sizes (from 120 × 120 m to 570 × 570 m) of 2017 were used to analyze the relationship between land-use composition and LST by performing a regression analysis. Based on these relationships, a multivariate regression model was derived for the prediction of LST from the land-use composition data. According to the European Green Capital report [39], the number of houses located at a distance of more than 300 m from a 0.5 ha adjacent green (or larger) is considered as a basis for the evaluation of a green city. If this number is large, the green score of the city will be reduced. It means that the smallest urban area used for evaluation is around 28 ha (=3.14 × 300 m^2). In addition, the Ministry of Construction of Vietnam issued a Circular No. 10/2008/TT-BXD to guide the assessment and recognition of model new urban centers on 22 April 2008. In the Circular, the first requirement is that the urban area must be 50 ha or more. We assumed that a window size of 510 × 510 m, 17 × 17 pixels of Landsat 8 image, close to 25 ha (a half of the minimum requirement of the Circular No. 10) can be considered representative enough as a suitable unit for urban land management and planning. The performance of the newly derived regression model with a 510 × 510 m window size was assessed for the prediction of LST with different window sizes. The model was validated with the statistical datasets of the hottest day of 2016. Implications of the derived regression model for urban planning and design were discussed. The outline of the research flowchart is shown in Figure 3.

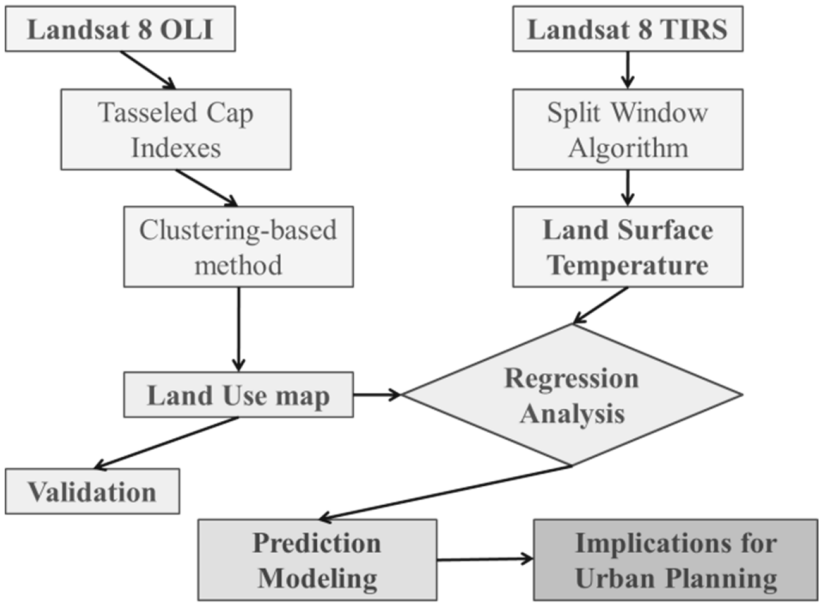

Figure 3. Outline of the research flowchart.

3. Results and Discussion

3.1. Land Use Maps, Land Use Changes, and Validation Results

The produced 30 m resolution land use maps of Hanoi for the years 2016 and 2017 are displayed in Figure 4a,b, respectively. Some areas with substantial land use changes are visually chosen and labeled as A, B, C, E, and F in Figure 4c,d, with coverage percentage statistics for the three major types of land use of concern in the years 2016 and 2017, respectively. The three major land-use types include built-up areas, vegetation covers, and water bodies. It is found that the changes in land-use coverage percentage are 4.4%, −4.4%, −0.8%, and 0.8% for built-up, vegetation, water, and others, respectively, from years 2016 to 2017. The 4.4 % area of inner Hanoi City is equivalent to 704 ha (7.04 km^2). Obviously, the increase in built-up area is mainly contributed by the decrease in vegetation coverage by 4.4%. However, it does not mean that built-up area is completely transformed from vegetation cover, since there are other minor land use covers. Even though we only consider the land-use changes in a one year interval from 2016 to 2017, the fast change of land use in inner Hanoi City is obvious by comparing the two consecutive years of images.

After the quantified areas of land use changes, qualitative land use changes may be easily observed by comparing the Google Earth images, which are conveniently available online, as well as field survey photos, as shown in Figure 5. Field survey photos were taken on 14 October 2018. The transformation of vegetation cover into built-up areas is easily detected by bare eyes. Figure 5a shows Google Earth image of Inner Hanoi City with areas B and E for the demonstration of land use changes and (red) dots with field survey photos as the ground truth for reference. Figure 5b,c are Google Earth images of area B that were acquired in June 2016 and August 2017, respectively, with four field survey photos showing the current in-situ land use status. Figure 5d,e are Google Earth images of area E, acquired in June 2016 and August 2017, respectively, with two field survey photos confirming the current in situ land use status of either built-up or ongoing construction circumstances.

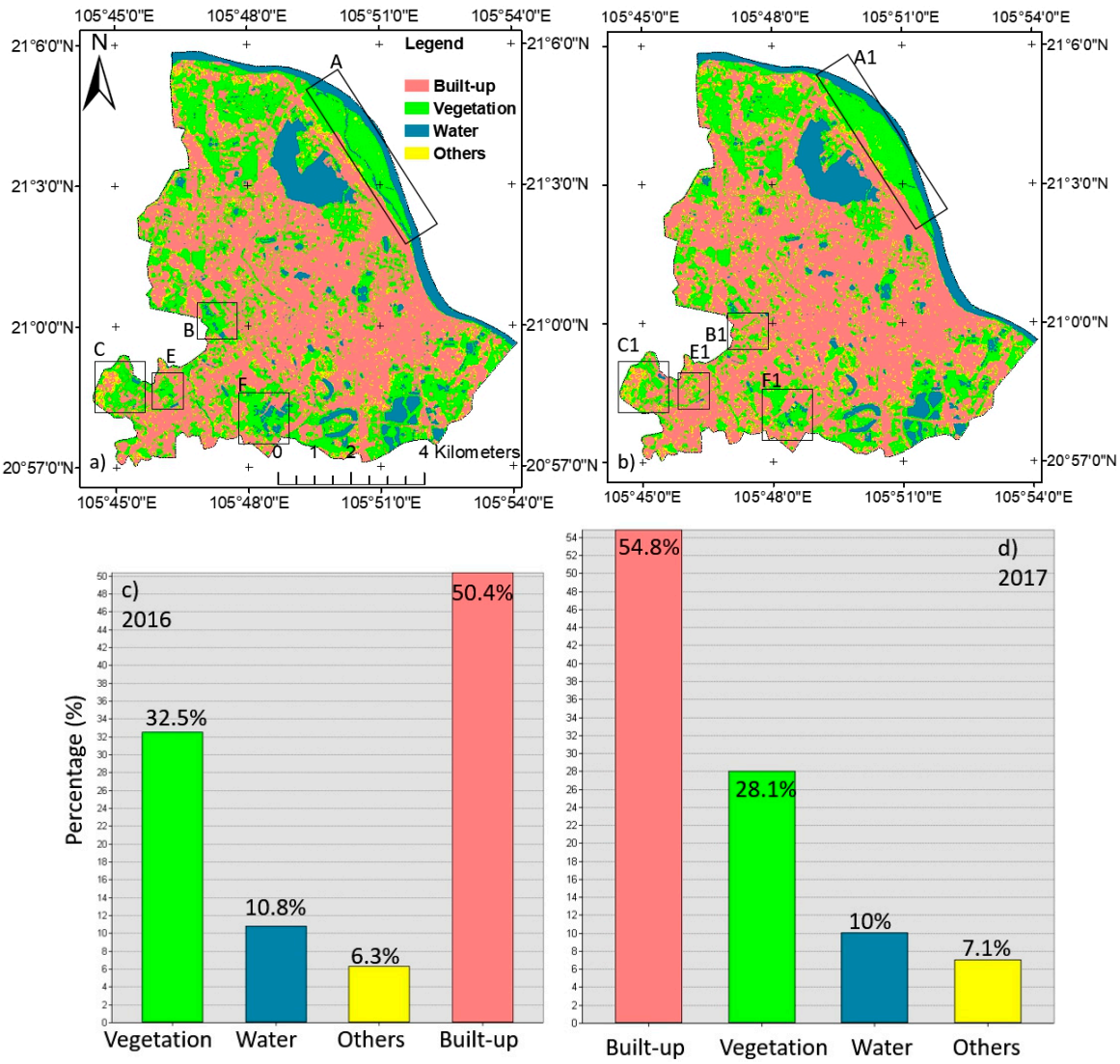

Figure 4. Land-use maps of inner Hanoi city for (**a**) 1 June 2016, and (**b**) 4 June 2017. Areas with substantial land-use changes are visually chosen and labeled as A, B, C, E, and F in (**c**) and (**d**) with coverage percentage statistics for the three major land-use types of concern and others in the years 2016 and 2017, respectively.

The accuracy assessment of LULC classification was performed to quantitatively assess how effective the pixels were sampled into the correct LULC classes. The accuracy assessment of pixel selection was on areas that could be clearly identified on both Landsat high-resolution images, and on Google Earth and Google Map. A total of 300 points (locations) for both years 2016 and 2017 were created in classification images of the study area, as presented in Section 2.4. The study had an overall classification accuracy of 92%, a kappa coefficient (K) of 0.88, an overall accuracy of 93%, and kappa coefficient (K) of 0.9, 0 for 2016 and 2017, respectively. The confusion matrices of LULC classification maps derived from Landsat 8 images in 2016 and 2017 are shown in Tables 3 and 4, respectively. The kappa coefficient is rated as being substantial, and hence, the classified image was found to be appropriate for further analysis.

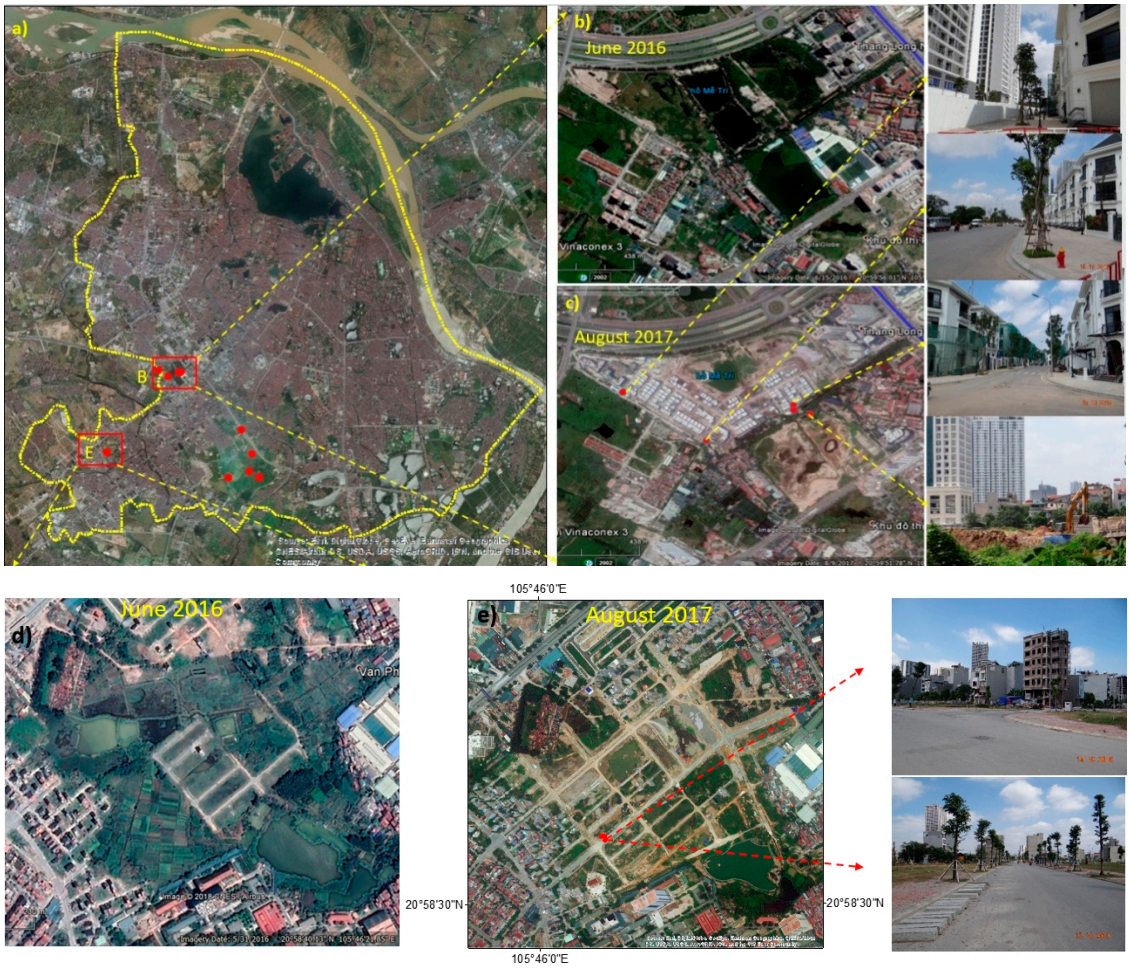

Figure 5. Field survey photos taken on 14 October 2018 are overlaid onto Google Earth images. (**a**) Google Earth image of Inner Hanoi City with areas B and E for the demonstration of land use changes and (red) dots with field survey photos as the ground truth for reference; (**b**,**c**) are Google Earth images of area B acquired in June 2016 and August 2017, respectively, with four field survey photos confirming the current built-up status; (**d**,**e**) are Google Earth images of area E acquired in June 2016 and August 2017, respectively, with two field survey photos confirming the current built-up status and on-going construction circumstances.

Table 3. Confusion matrix of land-use map classified from the Landsat 8 image in 2016.

Classified	Reference Data				Total (Pixels)	User's Accuracy
	Built-up	Vegetation	Water	Others		
1. Built-up	108	3	2	1	114	95%
2. Vegetation	5	95	2	0	102	93%
3. Water	4	1	62	0	67	93%
4. Others	2	3	1	11	17	65%
Total (pixels)	119	102	67	12	300	
Producer's accuracy	91%	93%	93%	92%		
Overall accuracy: 92%					Kappa coefficient: 0.88	

Table 4. Confusion matrix of land-use map classified from the Landsat 8 image in 2017.

Classified	Reference Data				Total (Pixels)	User's Accuracy
	Built-up	Vegetation	Water	Others		
1. Built-up	112	3	2	1	118	95%
2. Vegetation	5	94	1	0	100	94%
3. Water	4	1	62	0	67	93%
4. Others	2	2	0	11	15	73%
Total (pixels)	123	100	65	12	300	
Producer's accuracy	91%	94%	95%	92%		
Overall accuracy: 93%					Kappa coefficient: 0.90	

Table 5 shows the land-use classification and its changes from years 2016 to 2017 in inner Hanoi City. It reveals a big increase for built-up areas by 8.9% in a year, but a decrease for vegetation, water, and others by 10.9%, 7.0%, and 4.0%, respectively. For assessing the quantity of transformations among land-use types from the years 2016 to 2017, a transformation matrix is determined, as shown in Table 6. Two key points are observed from the table. First, increased built-up area 841 ha is primarily changed from vegetation (618 ha), followed by others (137 ha) and water (86 ha). Second, the transformations of built-up to vegetation, water, and others are 0.33% (27/7937), 0.27% (22/7937), and 0.92% (74/7937), respectively.

Table 5. Land-use changes between years 2016 and 2017 in inner Hanoi.

Land-Use Types	Area in 2016 (ha)	Area in 2017 (ha)	Changed Area (ha) (%)
Built-up	8060	8778	718 (8.9%)
Vegetation	5067	4516	−551 (−10.9%)
Water	1726	1605	−121 (−7.0%)
Others	1149	1103	−46 (−4.0%)
Total	16,002	16,002	0

Table 6. Transformation among land use types from years 2016 and 2017 in inner Hanoi.

Land-Use Types in 2016 (ha)	Land-Use Types in 2017 (ha)				
	Built-up	Vegetation	Water	Others	Total
Built-up	7937	27	22	74	8060
Vegetation	618	4051	41	357	5067
Water	86	87	1535	18	1726
Others	137	351	7	654	1149
Total	8778	4516	1605	1103	16,002

It is evident that, under the Master Plan 2030, the inner Hanoi City has been changing quickly with time, since the implementation of the Plan in 2011. This can be easily justified by the dramatic land cover changes in a year, by comparing the land-use maps of years 2016 and 2017. Under such a fast-changing land-use situation, any suggested measures for mitigation of UHI for the inner Hanoi City are urgently required.

3.2. Land Surface Temperature Maps

Figure 6 shows LST maps of the inner Hanoi City for (a) 1 June 2016 and (b) 4 June 2017, and their corresponding histogram distributions in (c) and (d), respectively. Three areas with substantial changes in LST are randomly chosen and labeled as B, E, and F in both (a) and (b) for a further interpretation of SUHI intensity's variation. It is found that the average LSTs are 40.9 °C and 40.1 °C for 1 June 2016 and 4 June 2017, respectively. That is, the average LST was slightly higher for the hottest days in 2016 than

2017 by 0.8 °C. Note that even with an overall warmer thermal environment for the whole of inner Hanoi City in 2016 than 2017, LSTs were lower in the areas with significant transformation of land-use from vegetation cover to built-up, labeled as B, E, and F, in 2016 than 2017 by 0.9, 0.8, and 2.5 °C, respectively. The number of pixels and mean LST for the three chosen areas B, E, and F on the two hottest days in 2016 and 2017 and the difference in LST between the two hottest days are shown in Table 7. Results indicate that the transformation of land-use from vegetation to built-up has enhanced the contrast in thermal signatures, i.e., LSTs, by 1.7, 1.6, and 3.3 °C in the three fast-changing land-use regions B, E, and F, respectively, in one year between years 2016 and 2017. The contrast confirms the cooling effect of vegetation cover on the SUHI intensity that cannot be overstressed in the hot urban cites.

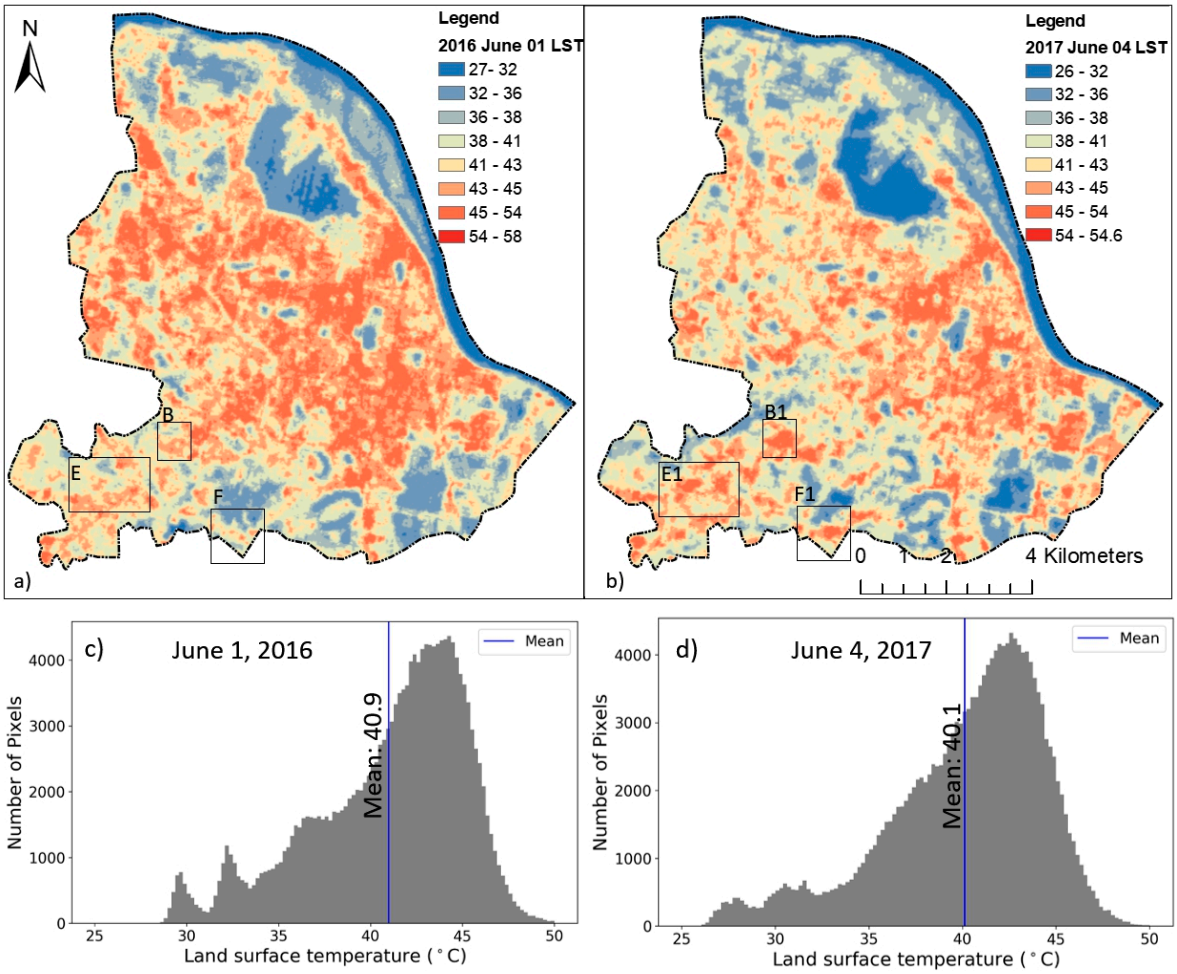

Figure 6. Land surface temperature (LST) maps of inner Hanoi City for (**a**) 1 June 2016 and (**b**) 4 June 2017; and their corresponding histogram distributions in (**c**,**d**), respectively. Three areas with substantial changes in LST between two hottest days are randomly chosen and labeled as B, E, and F in both (**a**,**b**). The pixel size is 30 × 30 m.

Table 7. Number of pixels (1 pixel = 30 × 30 m) and mean LST for the three randomly chosen areas B, E, and F on the two hottest days in 2016 and 2017, and the difference in LST between the two hottest days.

Zones	Number of Pixels	MEAN LST (°C)		Difference of LST (°C)
		June 2016	June 2017	
B-B1	800	43.4	44.3	0.9
E-E1	2386	40.9	41.7	0.8
F-F1	1791	38.3	40.8	2.5

As for the signature of the traditionally defined SUHI, it is analyzed here by assuming the boundary of Hanoi's downtown, that consists of seven districts, including Tay Ho, Hoan Kiem, Ba Dinh, Dong Da, Hai Ba Trung, Cau Giay, and Thanh Xuan Districts, as a mask to divide the urban (pink color) and suburban areas (green color), as shown in Figure 7. The statistics of urban and suburban LSTs are given in Table 8. The STDs in Table 8 represent the standard deviations of the LSTs retrieved from Landsat 8 images with a spatial resolution of 30 m.

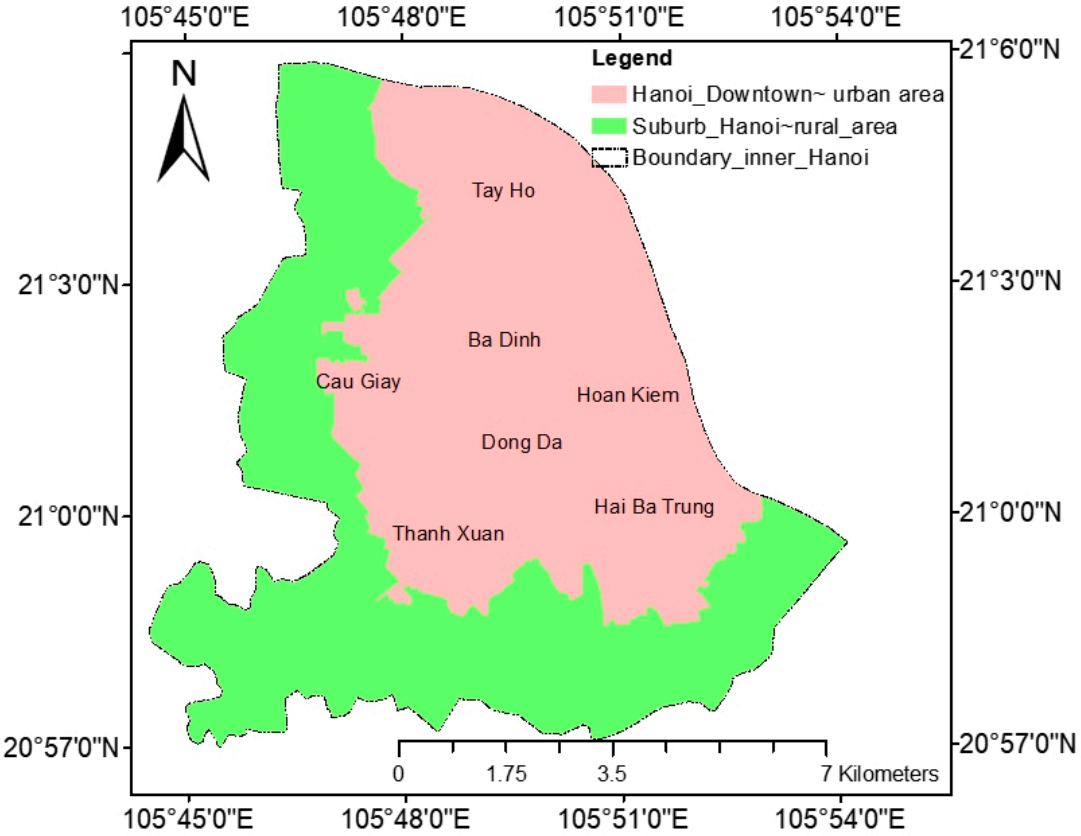

Figure 7. The map shows downtown of inner Hanoi (pink color) and suburban (green color).

Table 8. LSTs of urban and suburban areas of inner Hanoi. STD stands for standard deviation.

Areas	Mean LST (°C)/STD 2016	Mean LST (°C)/STD 2017	Number of Pixels
Urban	41.20/4.7	40.03/4.8	95463
Suburban	40.67/3.5	40.24/3.6	81792
LST anomaly (urban-suburban)	0.53	−0.21	

Table 8 indicates the mean LST of the urban area was higher by 0.53 °C than that in the suburban area in 2016. In contrast, in 2017, the LST of the urban area was lower than that in the suburban area, by 0.21 °C. This was due to the massive land use change in the suburban area, possibly resulting from the implementation of Hanoi Master Plan 2030, where many buildings are being constructed. That is, areas with vegetation and water surfaces in the suburban area are significantly reduced. Table 9 shows that the built-up area is increased by 4.28 km^2 and vegetation decreased by 4.01 km^2 in the suburban belt in only a one year interval from 2016 to 2017. Consequently, fast urbanization in suburban area results in slightly higher LSTs in the suburban area than in urban area in 2017. This finding is also in line with the comparative results of the LST in the chosen areas B, E, and F, which are located in the suburban belt to demonstrate a negative SUHI in response to urban expansion in inner Hanoi City.

Table 9. Land use/land cover (LULC) change in urban and suburban areas of Hanoi in 2016–2017.

	Built-up	Vegetation	Water	Others
LULC in suburban area 2016 (km^2)	33.22	28.95	5.59	6.01
LULC in suburban area 2017	37.50	24.93	4.73	6.61
Change LULC in suburban (2017–2016)	4.28	−4.01	−0.86	0.59
LULC in urban area 2016 (km^2)	47.29	22.90	11.65	4.07
LULC in urban area 2017	50.18	19.77	11.30	4.66
Change LULC in urban area (2017–2016)	2.89	−3.13	−0.35	0.59

3.3. Individual Land Use Coverage versus LST

Results from the regression analysis show that there exist high correlations between the percentage coverage of the individual land-use types (%U, %V, and %W) and the mean LSTs (μLSTs) for all window sizes considered in the research. However, in our study area, we detect that smaller window sizes (less than 300 × 300 m) do not properly represent a heterogeneous mixture of the land-use composition. In most cases, one or two components of the land-use composition (%W, %U, and %V) are absent. Therefore, we present the analysis results pertaining to window sizes of larger than 300 × 300 m. On the other hand, the correlations between the percentage coverage of the land use types (%U, %V, and %W) and μLSTs are much stronger for large than for small window sizes.

Figure 8 demonstrates the relationships between the percentage coverage of the land-use types (%U, %V, and %W) and μLSTs in the case of 510 × 510 m window size on the hottest day of 2017. The regression coefficients are found to be the highest for the water coverage (%W) with R^2 = 0.70, followed by urban built-up cover (%U), with R^2 = 0.67, and then vegetation cover (%V), with R^2 = 0.43. Note that water (%W) and vegetation (%V) coverages display negative correlations with μLST, as they play a known cooling effect on the SUHI intensity, whereas urban built-up coverage (%V) is positively correlated with μLST to enhance the UHI phenomena.

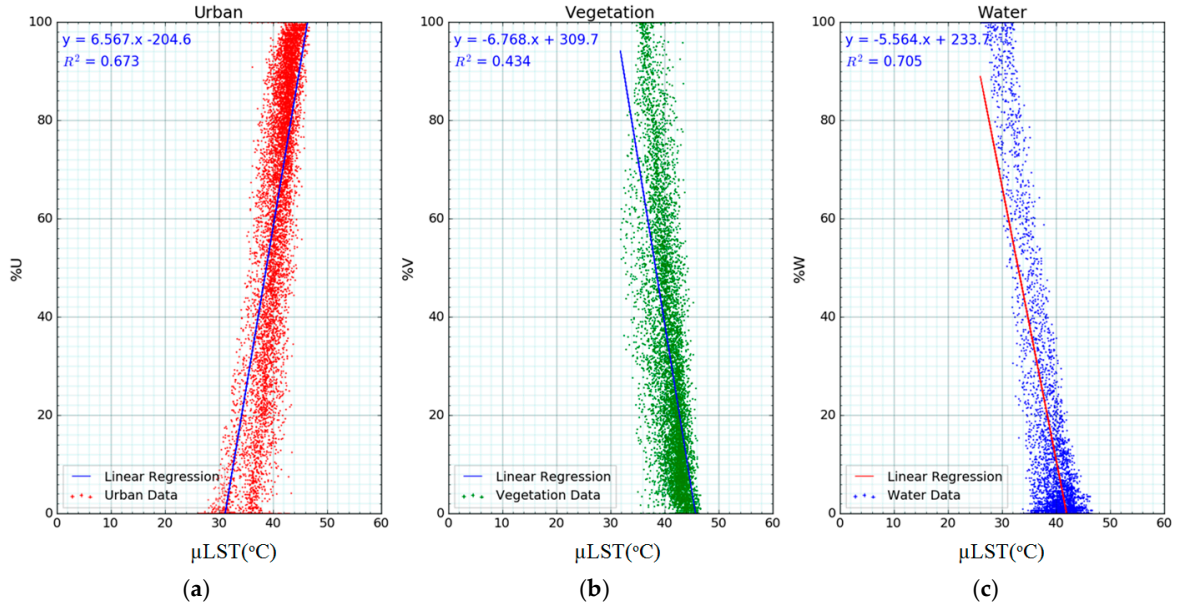

Figure 8. Relationships between percentage coverage of land-use types (%U, %V, and %W) and mean LSTs (μLST) on the hottest day of 2017 (4 June): (**a**) Urban coverage (%U); (**b**) Vegetation coverage (%V); and (**c**) Water coverage (%W) versus μLST.

3.4. Land-Use Composition–Driven Prediction of LST

A multivariate regression model between land-use composition (percentage coverage of urban built-up area (%U), vegetation (%V), and water (%W)) and LST on the hottest day of 2017 (4 June)

is derived. For this purpose, we utilized a 510 × 510 m window size, close to 25 ha, assumed to be a suitable unit for urban land management and planning. The resultant regression function is given in Equation (4):

$$\text{LST} = 0.032261 \times \%\text{U} - 0.040953 \times \%\text{V} - 0.137770 \times \%\text{W} + 42.01 \quad (4)$$

The performance of the above derived regression model (Equation (4)) for a 25 ha land management unit is evaluated by comparing its predicted LST for different window sizes with that derived from Landsat-8 data (LST_{LS8}). It was found that the regression function gave reasonable results, with $R^2 \sim 0.9$ for all cases (window sizes from 300 × 300 m to 570 × 570 m). Almost 90% of the variation in LST can be predicted by the model for window sizes of 330 × 330 m and 510 × 510 m (Figure 9). Since the R^2 alone may not be sufficient to evaluate the performance and accuracy of a prediction model, the RMS error (RMSE) and the ratio between RMSE and the standard deviation (STD) of the Landsat 8 LST map after windowing and averaging, i.e., $\text{RMSE/STD\_LST}_{\text{LS8}}$, are also reported. Note that if the ratio between $\text{RMSE/STD\_LST}_{\text{LS8}}$ is lower than 0.5, the model can be considered reliable. It is found that the RMSE and $\text{RMSE/STD\_LST}_{\text{LS8}}$ for the window sizes of 510 × 510 m and 330 × 330 m are 1.77 °C, 0.38, and 1.83 °C, 0.4, respectively. Such statistics justify that the regression model that is derived by using the 510 × 510 m window size can be applied for the prediction of LST for the other window sizes as well.

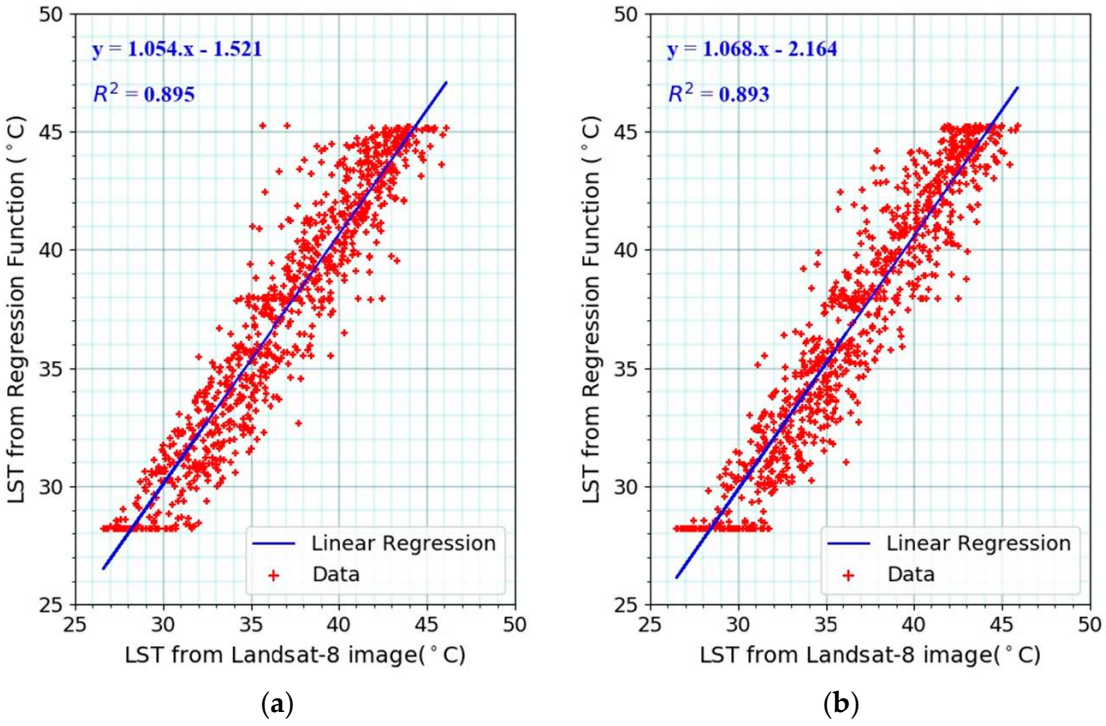

Figure 9. Land-use composition–driven predictions of LST for the hottest day of 2017 (4 June) versus LST observed by Landsat-8 for (**a**) 510 × 510 m and (**b**) 330 × 330 m window sizes.

3.5. Validation of the Land-Use Driven Model

We test the derived regression model (Equation (4)) for its predicted LSTs on another hottest day (1 June 2016) by using the statistical dataset of 2016. Figure 10 shows the land-use composition—driven predictions of LST for the hottest day of 2016 (1 June) versus the LST observed by Landsat-8 for (a) 510 × 510 m and (b) 330 × 330 m window sizes. High correlations of 0.897 and 0.869 for 510 × 510 m and 330 × 330 m window sizes, respectively, were obtained. RMSEs for the window sizes 510 × 510 m and 330 × 330 m were 1.71 °C and 1.94 °C, respectively. The ratios $\text{RMSE/STD\_LST}_{\text{LS8}}$ are also

low (below 0.5), at 0.44 and 0.5 for the window sizes 510 × 510 m and 330 × 330 m, respectively. They indicate that the regression model reasonably predicts the LST for the hottest day of 2016. That is, the developed model can be used to retrieve LST for the needs of land-use management and planning with high reliability.

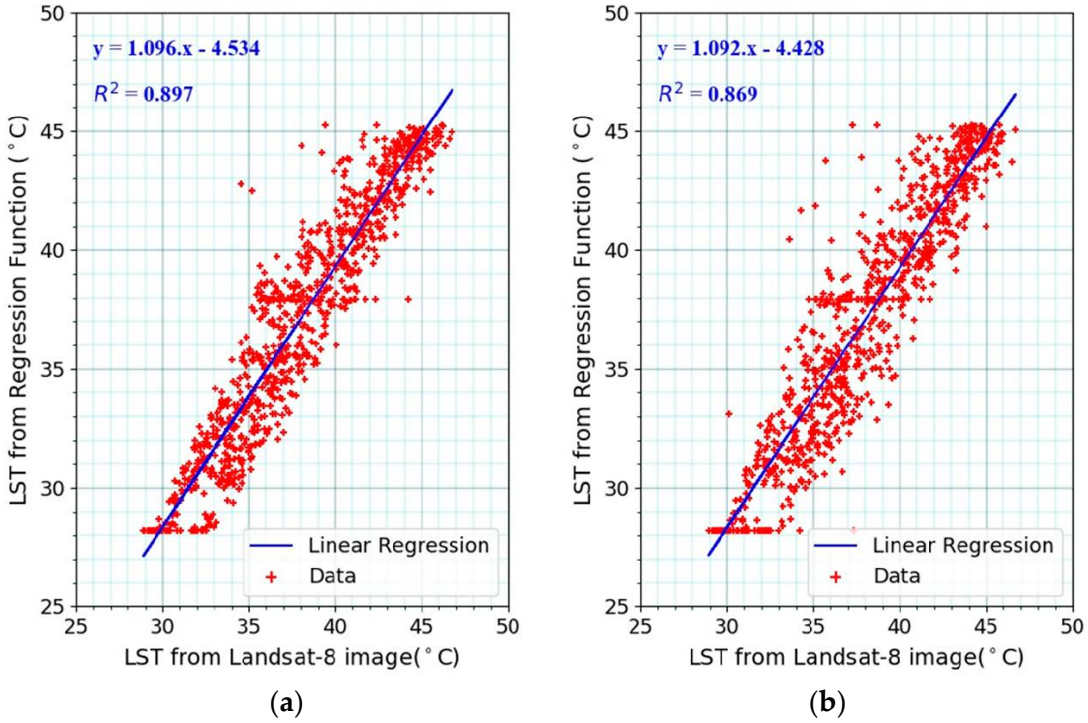

Figure 10. Land-use composition-driven predictions of LST for the hottest day of 2016 (1 June) versus LST observed by Landsat-8 for (**a**) 510 × 510 m and (**b**) 330 × 330 m window sizes.

4. Discussion

Hanoi is one of the hottest cities in Asia. It is highly vulnerable to the detrimental consequences of heat islands on urban ecology and human health. On 4 June 2017, Hanoi experienced a heat wave to the hottest level in recent 40 years, reaching 42 °C [40]. According to the study by Nguyen et al. [41], Vietnam's average temperature has increased at a rate of 0.26 °C per decade since the 1970s, which is approximately twice the rate of global warming over the same period of time. Over the last century, Hanoi has been experiencing a drastic increase in population, high-speed urbanization, and transformation of natural forests into urban built-up areas. All of these socioeconomic and biophysical changes have had a critical impact on the urban microclimate. As a result, severe heat waves have become common during the summer months in recent years. UHI is mainly caused by the modification of land surfaces and the concentration of the population [42]. The process of land modification generally increases the use of materials that retain heat (concrete surfaces) and sacrifices air-conditioning elements such as trees and water surfaces and moreover, waste heat is generated by energy usage [43]. In tropical cities, where there are a great number of very hot days, UHI causes the temperature to rise dramatically, negatively affecting the quality of the living environment in these cities.

By assuming that the unit of urban land management is around 25 ha (510 × 510 m), on a very hot day such as 4 June 2017, the LST (°C) can be predicted with respect to land-use composition using the regression model derived in this research, as shown in Table 10.

Table 10. Land-use composition-driven prediction of land surface temperature.

Land-Use Composition			LST (°C)
%U	%W	%V	
100	0	0	45.23
0	0	100	37.91
0	100	0	28.24
80	10	10	42.80
60	20	20	40.37

A substantial impact of land-use composition on LST and UHI is apparent from Tables 8 and 10. This analysis shows that the LST at each management unit (e.g., 25 ha) can be decreased from 45.23 °C (100% urban built-up cover) to 37.91 °C (100% vegetative cover), and then to 28.24 °C (100% water cover). The urban planner and designer indeed can neither change the LST directly to mitigate the UHI effects, and nor would it be possible to convert all urban built-up coverage in the cities to water bodies or vegetative areas. However, even a 20% conversion of urban built-up areas into vegetative (10%) and water bodies (10%) could reduce LST by 2.43 °C. The results of this research present an opportunity for urban planners and designers—the LST and associated effects of SUHI can be adjusted by managing the land-use composition and percentage coverage of the individual land-use types (%U, %V, and %W) in each urban land management unit. Reduction in the greenery has been described as a major cause of the rising temperature in cities by many researchers. It has been suggested that urban greening activities are the efficient nature-friendly solutions for mitigating UHI effects [44–46]. Such suggestions are also justified by the observed negative correlations between LST and NDVI, resulting in increased eco-environmental vulnerability [47–51].

5. Conclusion

We analyzed the correlations between land-use composition, the percentage coverage of three major land use types (%U, %V, and %W), and LST for different window sizes or urban land management units. The land use maps showed that inner Hanoi experienced substantial changes in land-use in a one-year interval from years 2016 to 2017, likely influenced by the City's Master Plan 2030. High correlations were observed between the percentage coverage of each land-use type (i.e., %U, %V, and %W) and LST. They are coherent with the findings of the previous studies, while considering different window sizes on the hottest day of 2017 (4 June). The vegetation and water coverages, acting as cooling effect, exhibited negative correlations with LST. In contrast, the urban coverage was proportionate to the LST. Consequently, a multivariate regression model was derived by taking into account the correlations between land-use composition and LST. We successfully validated our model for the prediction of LST on another hot day (1 June 2016). The validated model in this research provides an opportunity for urban planners and designers to suggest measures for adjusting the LST and the associated effects of SUHI by managing the land use composition and percentage coverage of the individual land-use types (%U, %V, and %W). This model demonstrates that a substantial decrease in LST can be achieved by increasing the proportion of vegetation and water for improved comfortable and sustainable living in the city. Despite this, we have provided some interesting findings, and we did not deeply analyze the traditionally-defined SUHI. In addition, impacts of currently rapid urbanization on SUHI and its consequence in suburban area of inner Hanoi can be further investigated.

Author Contributions: N.T.H. conceived the project, conducted research, performed initial analyses, and wrote the first manuscript draft. R.C.S. and D.D.C. provided helpful discussions during the conception of the project. D.-P.T. assisted in processing and analyses of data. K.-A.N. and Y.-A.L. enhanced the data processing, analysis, discussion, and conclusion. K.-A.N. and C.-L.L. improved the result presentation. Y.-A.L. rewrote around 70–80% of the first manuscript and finalized it for the first communication with the journal. Y.-A.L. and K.-A.N. implemented major revision to meet the standard of three anonymous reviewers.

Funding: Nguyen Thanh Hoan was funded by the Vietnam Academy of Science and Technology (VAST) under project code: VAST01.05/16-17, and Vietnam National Foundation for Science and Technology Development (NAFOSTED) under grant number 105.08-2015.31. K.A Nguyen and Y.A. Liou appreciate the financial support of Taiwan's Ministry of Science and Technology under project codes 105-2221-E-008-056-MY3, 107-2111-M-008-036 and 107-2622-E-008-006-CC3.

Acknowledgments: This research was assisted in collecting and processing of data from colleagues in Institute of Geography, VAST including: Ho Le Thu, Nguyen Van Dung and Hoa Thuy Quynh.

Conflicts of Interest: The authors declare no conflict of interest.

References

1. Howard, L. *The Climate of London Deduced from Meteorological Observations Made in the Metropolis and at Various Places around It (Electronic Resource)*; Harvey and Darton: London, UK, 1833.
2. Bornstein, R.D. Observations of the Urban Heat Island Effect in New York City. *J. Appl. Meteorol.* **1968**, *7*, 575–582. [CrossRef]
3. Ackerman, B. Temporal March of the Chicago Heat Island. *J. Clim. Appl. Meteorol.* **1985**, *24*, 547–554. [CrossRef]
4. Saitoh, T.S.; Shimada, T.; Hoshi, H. Modeling and simulation of the Tokyo urban heat island. *Atmos. Environ.* **1996**, *30*, 3431–3442. [CrossRef]
5. Kato, S.; Yamaguchi, Y. Analysis of urban heat-island effect using ASTER and ETM+ Data: Separation of anthropogenic heat discharge and natural heat radiation from sensible heat flux. *Remote Sens. Environ.* **2005**, *99*, 44–54. [CrossRef]
6. Kim, H.H. Urban heat island. *Int. J. Remote Sens.* **1992**, *13*, 2319–2336. [CrossRef]
7. Lin, C.Y.; Chen, W.-C.; Liu, S.C.; Liou, Y.A.; Liu, G.R.; Lin, T.H. Numerical study of the impact of urbanization on the precipitation over Taiwan. *Atmos. Environ.* **2008**, *42*, 2934–2947. [CrossRef]
8. Kar, S.K.; Liou, Y.A.; Ha, K.J. Characteristics of cloud-to-ground lightning activity over Seoul, South Korea in relation to urban effect. *Ann. Geophys.* **2007**, *25*, 2113–2118. [CrossRef]
9. Kar, S.K.; Liou, Y.A. Analysis of cloud-to-ground lightning and its relation with surface pollutants over Taipei, Taiwan. *Ann. Geophys.* **2014**, *32*, 1085–1092. [CrossRef]
10. Kar, S.K.; Liou, Y.A.; Ha, K.J. Aerosol effects on the enhancement of cloud-to-ground lightning over major urban areas of South Korea cloud-to-ground lightning over major urban areas of South Korea. *Atmos. Res.* **2009**, *92*, 80–87. [CrossRef]
11. Kar, S.K.; Liou, Y.A. Enhancement of cloud-to-ground Lightning activity over Taipei, Taiwan in relation to urbanization. *Atmos. Res.* **2014**, *147–148*, 111–120. [CrossRef]
12. Lin, C.Y.; Chen, F.; Huang, J.C.; Chen, W.C.; Liou, Y.A.; Chen, W.N. Urban heat island effect and its impact on boundary layer development and land-sea circulation over Northern Taiwan. *Atmos. Environ.* **2008**, *42*, 5639–5649. [CrossRef]
13. Weng, Q.; Lu, D.; Schubring, J. Estimation of land surface temperature-vegetation abundance relationship for urban heat island studies. *Remote Sens. Environ.* **2004**, *89*, 467–483. [CrossRef]
14. Chen, X.-L.; Zhao, H.-M.; Li, P.-X.; Yin, Z.-Y. Remote sensing image-based analysis of the relationship between urban heat island and land use/cover changes. *Remote Sens. Environ.* **2006**, *104*, 133–146. [CrossRef]
15. Kotharkar, R.; Surawar, M. Land Use, Land Cover, and Population Density Impact on the Formation of Canopy Urban Heat Islands through Traverse Survey in the Nagpur Urban Area, India. *J. Urban Plan. Dev.* **2016**, *142*, 04015003. [CrossRef]
16. Yuan, F.; Bauer, M.E. Comparison of impervious surface area and normalized difference vegetation index as indicators of surface urban heat island effects in Landsat imagery. *Remote Sens. Environ.* **2007**, *106*, 375–386. [CrossRef]
17. Oke, T.R.; Maxwell, G.B. Urban heat island dynamics in Montreal and Vancouver. *Atmos. Environ.* **1975**, *9*, 191–200. [CrossRef]
18. Miao, S.; Chen, F.; LeMone, M.A.; Tewari, M.; Li, Q.; Wang, Y. An Observational and Modeling Study of Characteristics of Urban Heat Island and Boundary Layer Structures in Beijing. *J. Appl. Meteorol. Clim.* **2009**, *48*, 484–501. [CrossRef]

19. Estoque, R.C.; Murayama, Y.; Myint, S.W. Effects of landscape composition and pattern on land surface temperature: An urban heat island study in the megacities of Southeast Asia. *Sci. Total Environ.* **2017**, *577*, 349–359. [CrossRef]
20. Singh, P.; Kikon, N.; Verma, P. Impact of land use change and urbanization on urban heat island in Lucknow city, Central India. A remote sensing based estimate. *Sustain. Cities Soc.* **2017**, *32*, 100–114. [CrossRef]
21. Schwarz, N.; Schlink, U.; Franck, U.; Großmann, K. Relationship of land surface and air temperatures and its implications for quantifying urban heat island indicators—An application for the city of Leipzig (Germany). *Ecol. Indic.* **2012**, *18*, 693–704. [CrossRef]
22. Dihkan, M.; Karsli, F.; Guneroglu, A.; Guneroglu, N. Evaluation of surface urban heat island (SUHI) effect on coastal zone: The case of Istanbul Megacity. *Ocean Coast. Manag.* **2015**, *118*, 309–316. [CrossRef]
23. Haashemi, S.; Weng, Q.; Darvishi, A.; Alavipanah, S. Seasonal Variations of the Surface Urban Heat Island in a Semi-Arid City. *Remote Sens.* **2016**, *8*, 352. [CrossRef]
24. Meng, Q.; Zhang, L.; Sun, Z.; Meng, F.; Wang, L.; Sun, Y. Characterizing spatial and temporal trends of surface urban heat island effect in an urban main built-up area: A 12-year case study in Beijing, China. *Remote Sens. Environ.* **2018**, *204*, 826–837. [CrossRef]
25. Gallo, K.; Hale, R.; Tarpley, D.; Yu, Y. Evaluation of the Relationship between Air and Land Surface Temperature under Clear- and Cloudy-Sky Conditions. *J. Appl. Meteorol. Clim.* **2011**, *50*, 767–775. [CrossRef]
26. Mutiibwa, D.; Strachan, S.; Albright, T. Land Surface Temperature and Surface Air Temperature in Complex Terrain. *IEEE J. Sel. Top. Appl. Earth Obs. Remote Sens.* **2015**, *8*, 4762–4774. [CrossRef]
27. Deilami, K.; Kamruzzaman, Md.; Liu, Y. Urban heat island effect: A systematic review of spatio-tempoal factors, data, methods, and mitigation measures. *Int. J. Appl. Earth Obs. Geoinf.* **2018**, *67*, 30–42. [CrossRef]
28. Lai, J.; Zhan, W.; Huang, F.; Quan, J.; Hu, L.; Gao, L.; Ju, W. Does quality control matter? Surface urban heat island intensity variations estimated by satellite-derived land surface temperature products. *ISPRS J. Photogramm. Remote Sens.* **2018**, *139*, 212–227. [CrossRef]
29. Li, H.; Zhou, Y.; Li, X.; Meng, L.; Wang, X.; Wu, S.; Sodoudi, S. A new method to quantify surface urban heat island intensity. *Sci. Total Environ.* **2018**, *624*, 262–272. [CrossRef]
30. Nam, T.H.H.; Kubota, T.; Trihamdani, A.R. Impact of Urban Heat Island under the Hanoi Master Plan 2030 on Cooling Loads in Residential Buildings. *Int. J. Built Environ. Sustain.* **2015**, *2*, 48–61. [CrossRef]
31. Trihamdani, A.R.; Lee, H.S.; Kubota, T.; Phuong, T.T.T. Configuration of Green Spaces for Urban Heat Island Mitigation and Future Building Energy Conservation in Hanoi Master Plan 2030. *Buildings* **2015**, *5*, 933–947. [CrossRef]
32. Baig, M.H.A.; Zhang, L.; Shuai, T.; Tong, Q. Derivation of a tasselled cap transformation based on Landsat 8 at-satellite reflectance. *Remote Sens. Lett.* **2014**, *5*, 423–431. [CrossRef]
33. Wang, Y. and E. Lentilucci. A Practical Approach to Landsat 8 TIRS Stray Light Correction Using Multi-Sensor Measurements. *Remote Sens.* **2018**, *10*, 589. [CrossRef]
34. García-Santos, V.; Cuxart, J.; Martínez-Villagrasa, D.; Jiménez, M.A.; Simó, G. Comparison of Three Methods for Estimating Land Surface Temperature from Landsat 8-TIRS Sensor Data. *Remote Sens.* **2018**, *10*, 1450. [CrossRef]
35. Sobrino, J.A.; Raissouni, N. Toward remote sensing methods for land cover dynamic monitoring: Application to Morocco. *Int. J. Remote Sens.* **2000**, *21*, 353–366. [CrossRef]
36. Jimenez-Munoz, J.C.; Sobrino, J.A.; Skokovic, D.; Mattar, C.; Cristobal, J. Land Surface Temperature Retrieval Methods from Landsat-8 Thermal Infrared Sensor Data. *IEEE Geosci. Remote Sens. Lett.* **2014**, *11*, 1840–1843. [CrossRef]
37. Yu, X.; Guo, X.; Wu, Z. Land Surface Temperature Retrieval from Landsat 8 TIRS—Comparison between Radiative Transfer Equation-Based Method, Split Window Algorithm and Single Channel Method. *Remote Sens.* **2014**, *6*, 9829–9852. [CrossRef]
38. NASA's Atmospheric Correction Parameter Calculator. Available online: http://atmcorr.gsfc.nasa.gov/ (accessed on 5 December 2018).
39. European Green Capital Report: Green Urban Spaces with Integration of Sustainable Land Use. Available online: http://ec.europa.eu/environment/europeangreencapital/wp-content/uploads/2016/12/Indicator-3-Green-urban-areas_Nijmegen-2018-revised.pdf (accessed on 11 November 2018).

40. VOV News: Vietnam Records Hottest Day So Far This Year in Capital of Hanoi. Available online: http://english.vov.vn/society/vietnam-records-hottest-day-so-far-this-year-in-capital-of-hanoi-350997.vov (accessed on 21 April 2018).
41. Nguyen, D.-Q.; Renwick, J.; McGregor, J. Variations of surface temperature and rainfall in Vietnam from 1971 to 2010: Variations of surface temperature and rainfall in Vietnam. *Int. J. Clim.* **2014**, *34*, 249–264. [CrossRef]
42. Zhou, D.; Bonafoni, S.; Zhang, L.; Wang, R. Remote sensing of the urban heat island effect in a highly populated urban agglomeration area in East China. *Sci. Total Environ.* **2018**, *628–629*, 415–429. [CrossRef] [PubMed]
43. Solecki, W.D.; Rosenzweig, C.; Parshall, L.; Pope, G.; Clark, M.; Cox, J.; Wiencke, M. Mitigation of the heat island effect in urban New Jersey. *Environ. Hazards* **2005**, *6*, 39–49. [CrossRef]
44. Rotem-Mindali, O.; Michael, Y.; Helman, D.; Lensky, I.M. The role of local land-use on the urban heat island effect of Tel Aviv as assessed from satellite remote sensing. *Appl. Geogr.* **2015**, *56*, 145–153. [CrossRef]
45. Kardinal Jusuf, S.; Wong, N.H.; Hagen, E.; Anggoro, R.; Hong, Y. The influence of land use on the urban heat island in Singapore. *Habitat Int.* **2007**, *31*, 232–242. [CrossRef]
46. Tang, J.; Di, L.; Xiao, J.; Lu, D.; Zhou, Y. Impacts of land use and socioeconomic patterns on urban heat Island. *Int. J. Remote Sens.* **2017**, *38*, 3445–3465. [CrossRef]
47. Lin, P.; Lau, S.S.Y.; Qin, H.; Gou, Z. Effects of urban planning indicators on urban heat island: A case study of pocket parks in high-rise high-density environment. *Landsc. Urban Plan.* **2017**, *168*, 48–60. [CrossRef]
48. Keeratikasikorn, C.; Bonafoni, S. Urban Heat Island Analysis over the Land Use Zoning Plan of Bangkok by Means of Landsat 8 Imagery. *Remote Sens.* **2018**, *10*, 440. [CrossRef]
49. Nastran, M.; Kobal, M.; Eler, K. Urban heat islands in relation to green land use in European cities. *Urban For. Urban Green.* **2018**. [CrossRef]
50. Nguyen, A.K.; Liou, Y.-A.; Li, M.H.; Tran, T.A. Zoning eco-environmental vulnerability for environmental management and protection. *Ecol. Indic.* **2016**, *69*, 100–117. [CrossRef]
51. Liou, Y.-A.; Nguyen, A.K.; Li, M.H. Assessing spatiotemporal eco-environmental vulnerability by Landsat data. *Ecol. Indic.* **2017**, *80*, 52–65. [CrossRef]